Journal of Applied Fluid Mechanics, Vol. 9, No. 5, pp. 2403-2411, 2016.
Available online at www.jafmonline.net, ISSN 1735-3572, EISSN 1735-3645.
DOI:10.18869/acadpub.jafm.68.236.24749

Dominant Vortex Structures in Transverse Jets

S. Bayraktar† and T. Yilmaz

Yildiz Technical University, Department of Naval Architecture and Marine Engineering, 34349 Istanbul, Turkey

†*Corresponding Author Email: sbay@yildiz.edu.tr*

(Received March 1, 2015; accepted December 1, 2015)

ABSTRACT

In this paper, formation and development of one of the most dominant vortex structures, namely, counter-rotating vortex pair (CVP) which is seen in the jet in crossflow are investigated numerically. Influences of the inclination angles between the nozzle(s) and channel on the CVP are presented for three inclination angles, α=30°, 60° and 90° at velocity ratio, R=2.0. Effects of the number of the nozzles on the evolution of CVP is analyzed by considering the single and three side-by-side positioned circular nozzles. In addition to the CVP, some secondary vortices are also reported by considered relatively a narrow channel because their existence cannot be showed in wider channel. Simulations reveal that higher the inclination angle the more jet penetration into the channel in all directions and increasing the inclination angle causes larger CVPs in size. Although the flow structure of the CVP formed in the single and three side-by-side nozzles are similar their evolution is quite different.

Keywords: Transverse jet; Turbulent flow; Counter-rotating vortex pair (CVP); Computational fluid dynamics (CFD).

NOMENCLATURE

CFD	computational fluid dynamics	V/STOL	vertical/short take off/landing
CVP	counter-rotating vortex pair	w	velocity components in z-direction
D	jet diameter	x-	streamwise direction
DNS	direct numerical simulation	y-	spanwise direction
H	height of the channel	y^+	non-dimensional distance from the center of the cell to the wall surface
JICF	jet in crossflow	z-	normal direction
k	turbulence kinetic energy		
L	length of the pipe		
LDA	laser doppler anemometer	α	inclination angle
LES	large eddy simulation	ε	turbulence kinetic energy dissipation rate
P	pressure	μ_t	turbulent viscosity
R	velocity ratio ($= w_j / u_{cf}$)	μ_{eff}	effective viscosity
RANS	Reynolds Averaged Navier-Stokes	α_k	inverse effective Prandtl numbers for k
Re	Reynolds number	α_ε	inverse effective Prandtl numbers for ε
SKE	standard k-epsilon		
SST	shear stress transport	Subscripts	
u	velocity components in x-direction	cf	crossflow
$\overline{u_i u_j}$	Reynolds stresses	j	jet
v	velocity components in y-direction		

1. INTRODUCTION

Most of the flows in the nature are turbulent. One of the turbulent flows seen in the nature is the JICF. The term "crossflow" is used for the main channel flow, in which the jet is injected from nozzle(s). JICF expresses the flow at which its direction is completely different from the crossflow. Free stream forces the jet flow to change its direction due to its momentum. JICF is encountered in various industrial and natural applications such as stack smoke, flow in combustion room, hypersonic

missile, rocket control systems, low mass flux boundary layer control systems to V/STOL aircrafts. The flow of transverse jet depends on various variables such as jet-to-crossflow momentum ratio and inclination angle; jet flow conditions such as subsonic/supersonic; cross flow conditions such as laminar, turbulent, subsonic/supersonic; jet nozzle geometry: square, parabolic, circular, etc. When a jet issuing into a cross flow, the jet bends quickly over in the direction of the crossflow and leads to a complex interaction between the jet and crossflow. Due to these interactions different vortex structures can be identified such as horse shoe, wake, shear layer vortices and CVP as shown in Fig. 1.

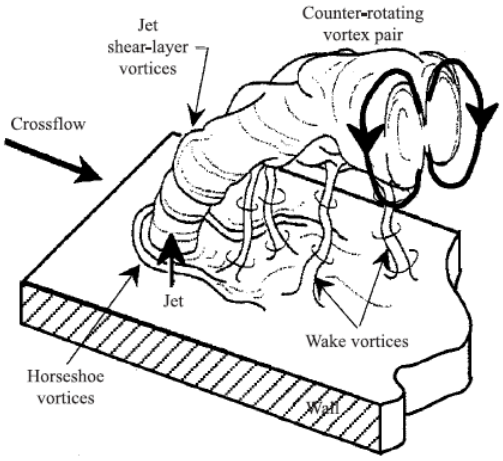

Fig. 1. Dominant vortex structures in JICF phenomenon (Fric and Roshko, 1994).

Due to its importance lots of papers which report computational and experimental results have been published so far. First of all, an extensive review of jet in crossflow for the period of 1943-1993 provided by Margason (1993) should be mentioned here. Effects of nozzle geometry have been investigated numerically by Foster and Engblom (2003) and Tomioka *et al*. (2003) for Mach number of 1.2 and 3.0, respectively. Hatch *et al*. (1992) and Hatch *et al*. (1995) performed series of studies to take into account the effect of the jet nozzle geometry on the flow and film cooling. As reported by Haven and Kurosaka (1997) at the vicinity of the jet and at relatively low velocity ratios, jet dynamics has an important role due to jet nozzle exit geometry.

Some researchers, for example Tyagi and Acharya (2000) investigated the effect of inclination angle on the diffusion and control of the transverse jets by using a rectangular nozzle. For this purpose two different inclination angles, 30° and 90° have been used. It was revealed that high inclination angle leads to more diffusion of the jet. It was also showed that at normal injection high pressure gradients might be dominated although it is not the case for the lower inclination angle. Fuller and Walters (1991), Williams and Hartfield (1996) and Wang (2000) used different inclination angle such as 25°, 35°, 45° and 60° revealing the velocity and vorticity fields. Most of reported studies on inclined jets dealt with the effects of inclination angle on the flow structure associated with film cooling phenomena such as Rowbury *et al*. (2001), Bayraktar and Yilmaz (2008), Renze *et al*. (2008) and Bayraktar and Yilmaz (2011).

One of the most significant vortex structure encountered in JICF phenomena is the CVP which begins to take form near the jet exit and becomes dominant in the far field. According to Andreopoulos and Rodi (1984), Fric and Roshko (1989), Fric and Roshko (1994), Kelso *et al*. (1996) and Cortelezzi and Karagozian (2001) CVP originates from the jet shear layer. Guo *et al*. (2006) proposed two major contributing sources such as the shearing effect between two different flows (jet and crossflow) and the vorticity contained in the wall layer of jet and crossflow.

Different explanations for the generation of CVP have been reported so far. For example Kamotani and Greber (1972) claimed that the CVP is formed in the wake region of the JICF due to the pressure gradient in the near hole region. Marzouk and Ghoniem (2007) concluded that the near field of the jet is dominated by deformation and periodic roll-up of the shear layer, results the CVP. Effects of the number of nozzles on the flow field is reported in the study of Huang (2015) which investigated the influence of the pressure ratio on the evolution of CVP by means of SST k-ω model for four square-shaped port holes.

As cited references on the topic reveals, most of the previous works report the evolution of the CVP for only one jet issued normal to the crossflow. To the author's knowledge, there has not been done any comprehensive computational works that investigated the effects of the inclination angle as well as the number of nozzle on the evolution of the CVP.

The paper has been divided into four parts. After a short discussion on JICF and an overview over the related literature, governing equations and numerical methods have been introduced in the second part. Flow configuration, boundary conditions and obtained results have been examined in third section. The final part presents the evolution and development of CVPs for various configurations.

2. MATHEMATICAL MODEL

2.1 Computational Domain

A better understanding of the flow field can be achieved if the problem is analyzed in 3D. Therefore, all simulations were performed on a 3D working domain that is designed to cover a rectangular channel extended 59D in the streamwise, 10D in the spanwise and 15D in the normal directions. The jet exit is at a distance 14D from the crossflow inlet plane (Fig. 2). For three side-by-side nozzle arrangement the computational

domain is extended to 14D in the spanwise direction to ensure that CVP develops independently without affected by the side walls. The computational domain consists of a cylindrical pipe (L_j=40D) and a rectangular duct with constant cross-sections. A detailed information on the working domain is given in Table 1.

Table 1 Dimension of the working domain

Geometry	Direction	Length
Channel	Streamwise (x)	x/D=-14…44
	Spanwise (y)	y/D=0…10
	Normal (z)	z/D=0…15
Jet	Streamwise (x)	x/D=-0.5D…0.5D
	Spanwise (y)	y/D=0…0.5D
	Normal (z)	z/D=-40…0

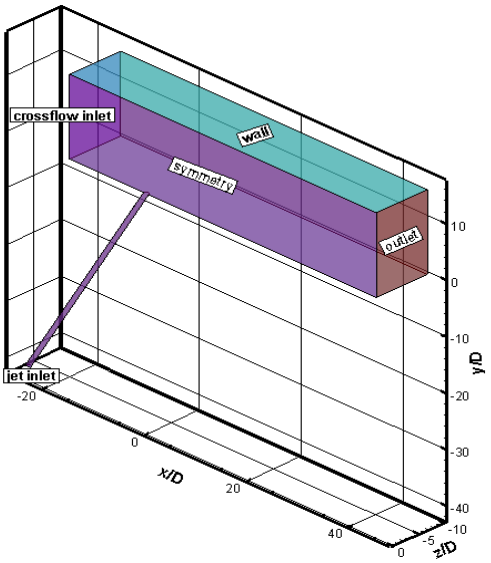

Fig. 2. Working domain for single nozzle.

2.2 Mesh Structure

Structured mesh with hexahedral elements is used for the decomposition of the flow field as shown in Fig. 3. Totally $242^x \times 60^y \times 70^z$ and $80^x \times 40^y \times 40^z$ grid points have been used for channel and the pipe, respectively.

Special attention was taken to the boundary layer region to obtain more accurate results since viscous forces are dominated at this region. Unlike the outer region of the boundary layer, denser mesh points have been generated near the wall to to ensure y^+=1. Totally 40 mesh elements have been used in the boundary layer to consider sharp gradient variations. As showed in Fig. 3 denser grids are preferred towards the pipe exit where jet flow and crossflow encounter.

2.3 Boundary Conditions

Crossflow is provided from –x to +x while jet is issued from a circular cross-sectional nozzle into the channel upward (from –y to +y). Therefore, these planes (yz and xz) were defined as velocity inlet. The right side of the channel was specified as pressure outlet while remaining boundaries were imposed as no-slip walls. To avoid using more mesh elements that apparently will increase the computational time, z/D=0.0 was specified as the symmetry plane.

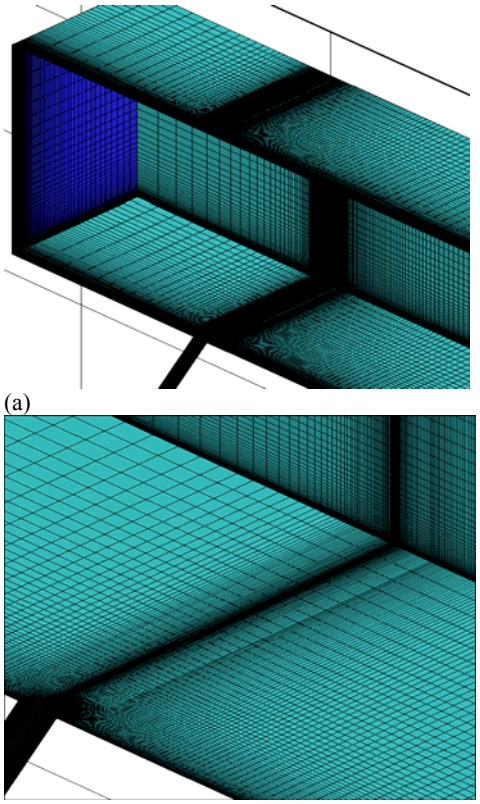

(a)

(b)

Fig. 3. Mesh structure, a) general view, b) Close-up view.

Reynolds numbers (Re) based on free stream velocity and channel length for crossflow and jet inlet velocity and pipe diameter for jet flow are shown in Table 2 with other corresponding values.

At the inlets of the channel and pipe uniform velocity profiles are prescribed. The distance between the leading edge of the channel and the pipe is kept sufficiently long to assure that the flow is fully developed till it encounters with the jet flow. The turbulent kinetic energy and its dissipation rate are specified using following equations (Eq.1-Eq.4) according to Demuren and Rodi, 1987.

$$k_j = 0.0020(w_j)^2 \tag{1}$$

$$k_{cf} = 0.00010(u_{cf})^2 \tag{2}$$

$$\varepsilon_j = \frac{k_j^{3/2}}{0.5 \times D} \tag{3}$$

$$\varepsilon_{cf} = \frac{k_{cf}^{3/2}}{0.2 \times H_{cf}} \tag{4}$$

Table 2 Corresponding values used in the simulations

Velocity Ratio	Channel (Crossflow)			Jet		
	u_{cf}	Re_{cf}	L_{cf}/D	w_j	Re_j	L_j/D
$R=w_j/u_{cf}$	(m/s)	-	-	(m/s)	-	-
1.4	5	1.88×10^5	59	7	4470	40
2.0	5	1.88×10^5	59	10	6386	40

2.4 Mathematical Equations and Turbulence Model

Numerical simulations of jet in crossflow problem include mainly two groups of approaches: The first one employs DNS or LES and the other approach uses RANS. As reported in the relevant literature DNS and LES have shown promising results but they are not currently employed for especially practical industrial applications widely because of the relatively large computer memory and CPU requirements. Performing a set of simulations to investigate the effects of various parameters on the development of CVP requires enormous computation time and computer sources such as memory and CPU. Since all simulations were performed on a Pentium 4 machine, 2.2 GHz preprocessor speed with 8 GB memory, it was not possible to employ LES or DNS. Based on these facts, prediction of jet penetration and development of CVP have been investigated numerically by using RANS solver. Lots of turbulence models are introduced for practical applications but none of them are usable for any type of problem. Coletti *et al*., 2013 reported that the formation mechanism of the CVP and its strength cannot be captured properly with standard SKE turbulence model due to overestimated eddy viscosity. Considering this result into account another version of k-ε turbulence model is chosen: Reliable k-ε (RKE) model (Shih *et al*., 1995).

As stated in detail by Cable, 2009 the RKE turbulence model has become one of the most widely used turbulence models due to its some advantages such as robustness and accuracy with respect to other versions of k-epsilon models. First of all, it uses an improved method for calculating the turbulent viscosity and secondly the dissipation rate is derived from the exact transport equation of the fluctuating component of vorticity, Bulat and Bulat, 2013. It is also recommended for the dissipation rate of flat and round jets which is successfully validated by the present computational work. The transport equations for the RKE model are given below:

$$\frac{\partial(\rho k)}{\partial t}+\frac{\partial}{\partial x_j}\left(\rho k u_j\right)=\frac{\partial}{\partial x}\left[\left(\mu+\frac{\mu_t}{\sigma_k}\right)\frac{\partial k}{\partial x_j}\right]+ G_k-\rho\varepsilon-Y_M \tag{5}$$

$$\frac{\partial(\rho\varepsilon)}{\partial t}+\frac{\partial}{\partial x_j}\left(\rho\varepsilon u_j\right)=\frac{\partial}{\partial x}\left[\left(\mu+\frac{\mu_t}{\sigma_\varepsilon}\right)\frac{\partial\varepsilon}{\partial x_j}\right]+\rho C_1 S\varepsilon-\rho C_2\frac{\varepsilon^2}{k+\sqrt{\nu\varepsilon}} \tag{6}$$

where

$$C_1=\max\left[0.43,\frac{\eta}{\mu+5}\right] \tag{7}$$

$$\eta=S\frac{k}{\varepsilon} \tag{8}$$

$$S=\sqrt{2S_{ij}Si_j} \tag{9}$$

In the above equations G_k represents the generation of turbulence kinetic energy due to the mean velocity gradients, Y_M represents the contribution of the fluctuating dilatation in compressible turbulence to the overall dissipation rate. C_2 and $C_{1\varepsilon}$ are constants and σ_k and σ_ε are the turbulent Prandtl numbers for k and ε, respectively. Their values are $C_{1\varepsilon}$=1.44, C_2=1.9, $\sigma_k=1.0$, $\sigma_\varepsilon=1.2$.

The eddy viscosity shown in Eq. 5 and Eq. 6 is computed from Eq. 10 as given below:

$$\mu_t=\rho C_\mu\frac{k^2}{\varepsilon} \tag{10}$$

where,

$$C_\mu=\frac{1}{A_0+A_s\frac{ku^*}{\varepsilon}} \tag{11}$$

$$u^*=\sqrt{S_{ij}S_{ij}+\tilde{\Omega}_{ij}\tilde{\Omega}_{ij}} \tag{12}$$

$$\tilde{\Omega}_{ij}=\Omega_{ij}-2\varepsilon_{ijk}\omega_k \tag{13}$$

$$\Omega_{ij}=\overline{\Omega_{ij}}-\varepsilon_{ijk}\omega_k \tag{14}$$

where $\overline{\Omega_{ij}}$ is the mean rate-of-rotation tensor viewed in a moving reference frame with the angular velocity ω_k.

The continuity and momentum equations are given in Eq. 10-16, respectively

$$\frac{\partial\rho}{\partial t}+\frac{\partial}{\partial x_j}\left(\rho u_j\right)=0 \tag{15}$$

$$\frac{\partial\rho u_i}{\partial t}+\frac{\partial}{\partial x_j}\left(\rho u_i u_j\right)=-\frac{\partial P}{\partial x_i}+\frac{\partial}{\partial x_j}\left[\mu\left(\frac{\partial u_i}{\partial x_j}+\frac{\partial u_j}{\partial x_i}\right)-\rho\overline{u_i u_j}\right] \tag{16}$$

Convergence to the steady-state solution is assessed by evaluating the value of the residuals of momentum and continuity equations as a function

of the iteration number. It is assumed that the computation has converged to the correct steady-state solution when the values of the residuals are lower than 10^{-05}.

2.5 Validation

To verify feasibility and asses the accuracy of the performance of the turbulence model employed in the present study, the computational procedures are validated with the experimental data of Kalifa *et al*., 2014 for R=1.4 (Fig. 4a) and Andreopoulos and Rodi, 1984 for R=2.0 (Fig. 4b).

Comparisons with the data of Kalifa *et al*., 2014 reveal that some discrepancies are occurred from y/D=0.0 to y/D=2.0. It is believed that this is due to the strong interactions between the crossflow and the jet flow because this is the region (x/D=-1.0-2.4) where two flows encounter to each other. However, at higher velocity ratio (R=2.0) the simulations are in good agreement with the results of the Andreopoulos and Rodi, 1984 except at x/D=2.0. It is clear that the CFD results and the experimental data are compared well at the subsequent stations towards the exit of the channel

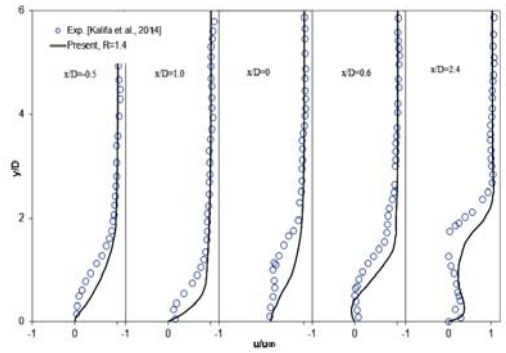

(a)

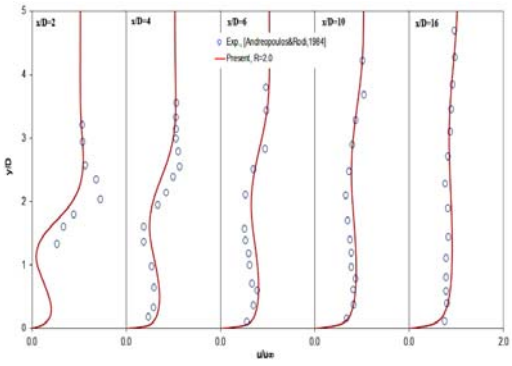

(b)

Fig. 4. Comparisons of the present results with the experimental data of a) Kalifa *et al*., 2014 and b) Andreopoulos and Rodi, 1984 for α=90°.

3. RESULTS AND DISCUSSION

It is observed that crossflow experiences three-dimensional separation around the nozzle because of the presence of the jet. When jet momentum is higher than the crossflow momentum, the jet pushes the crossflow in the lateral direction at the edge of the nozzle. This is the case when velocity ratio and inclination angles increases. In the present paper, complicated flow patterns are showed at various streamwise stations for different nozzle arrangements (single and side-by-side) and inclination angles for R=2.0. Although the results are presented for only one velocity ratio (R=2.0), simulations are performed for R=1.0 and R=1.4 especially for the validation of the simulations.

Effect of the inclination angles on the flow field at symmetry plane is shown in Fig. 5. Due to adverse pressure gradient and the injection of the jet into the crossflow different type of vortices are observed, except α=30°. At the inclination angle of α=30° the flow bends to the channel ground due to the strong momentum of the crossflow and flows over it. It can be seen that when inclination angle increases the jet penetrates deeper into the channel and tries to keep its trajectory. It stands as a rigid obstacle to the crossflow and blocks it. However, due to the entrainment effects of the jet the overall flow field is somewhat different from the flow over a rigid body.

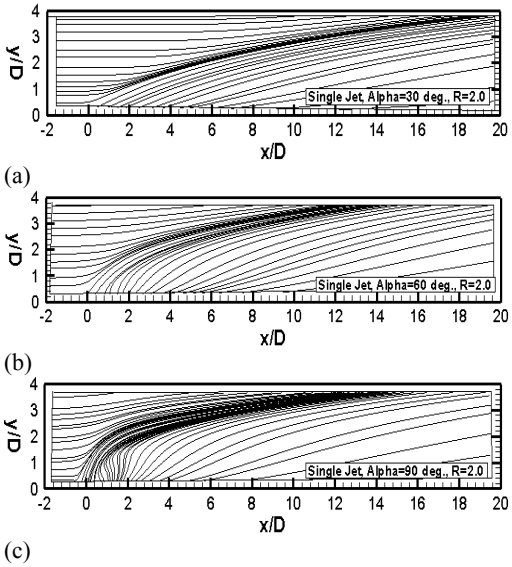

(a)

(b)

(c)

Fig. 5. Flow field at symmetry plane for inclination angle of a) α=30, b) α=60°, c) α=90° for R=2.0.

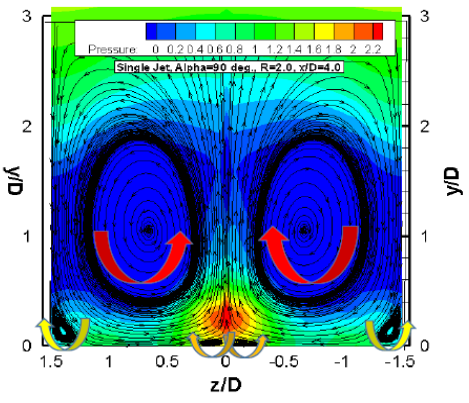

Fig. 6. Near-wall and secondary vortices.

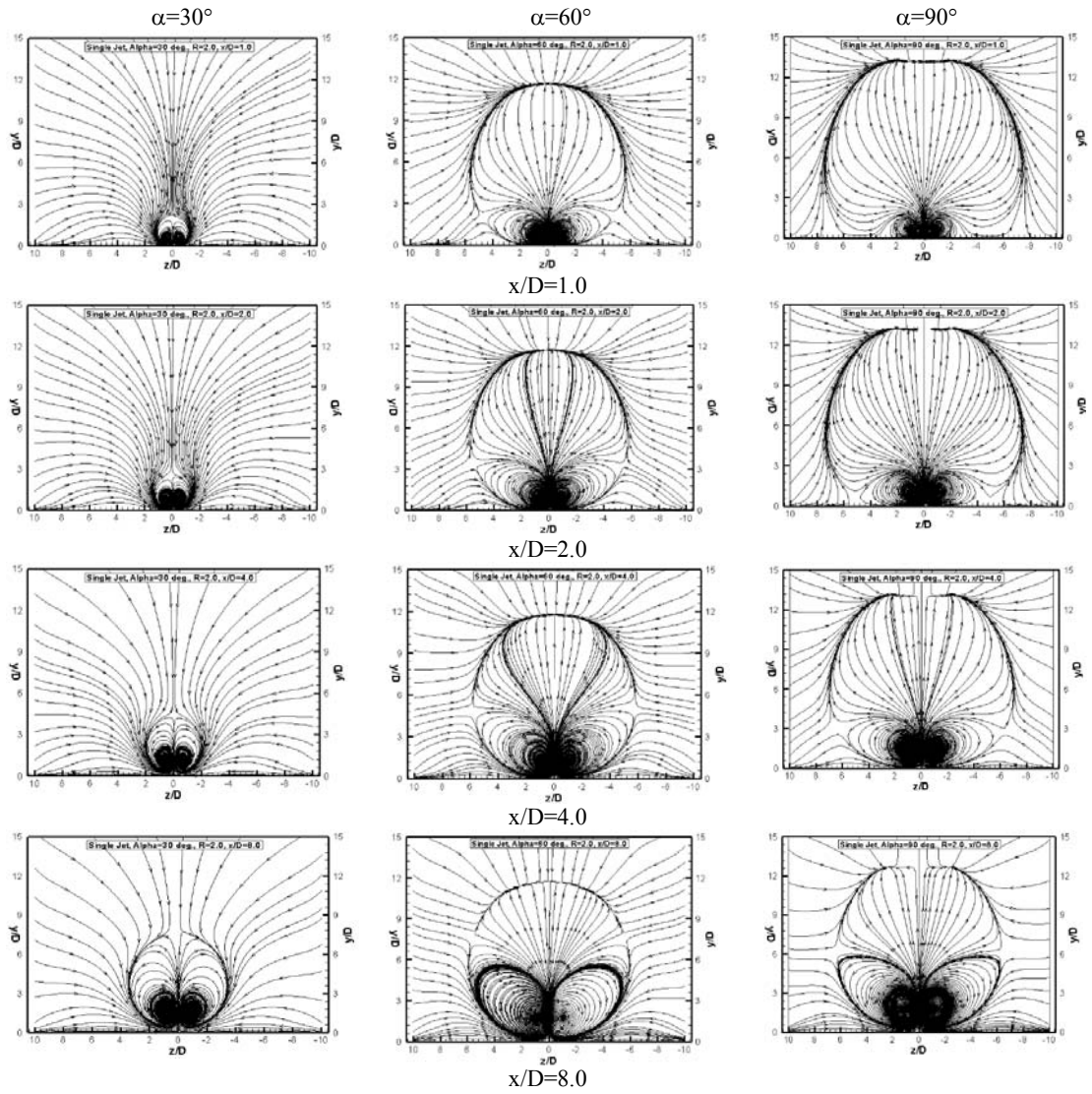

Fig. 7. CVP development at different inclination angles for the single nozzle arrangement, R=2.0.

The effects of the channel on the existence of the near-wall and secondary vortices showed in Fig. 1 by Fric and Roshko, 1994 are examined by decreasing the channel with.

It is observed that when a relatively narrow channel is used side walls affect not only the near-wall and secondary vortices but also change the evolution of the CVP. Two different secondary vortices are detected in the narrow channel. One of them is formed in the sides of the channel while the second type is visible in the center of the channel between the main CVP and the lower wall, Fig. 6.

Although, the development of the secondary vortices is similar to the main CVP, they rotate in the opposite direction of the main CVP. As inclination angle increases the secondary and near-wall vortices grow in size along with the streamwise direction. Near-wall secondary vortices grow with streamwise distance until they attain a limit width. Although not shown here, the near-wall vortices start to form at x/D=1.0 and grow until x/D=8.0 and then starts to decrease in size from x/D=12.0 before diminishes towards the channel exit. Meanwhile, the secondary vortices seen in the region between the ground and side walls of the channel keep their sizes after they reach their limits. It should be noted here that, such secondary vortices neither at the center of the channel (near-wall vortices) nor close to the channel walls cannot be detected in the wider channel.

Fig. 7 serves to depict the important structural differences due to the different inclination angles. It is observed that the CVP begins forming quite early. Especially at the first station and the lowest inclination angle it is seen that the cross section of the jet is nearly circular and it is located especially very close to the channel ground. Then, it grows and deforms from its initial circular shape into a distorted oval or kidney-like during its development at all inclination angles. It is realized that the CVP grows larger, spreads along with the y- and z-directions and finally occupies the entire channel. Vortex pair keeps its development through the

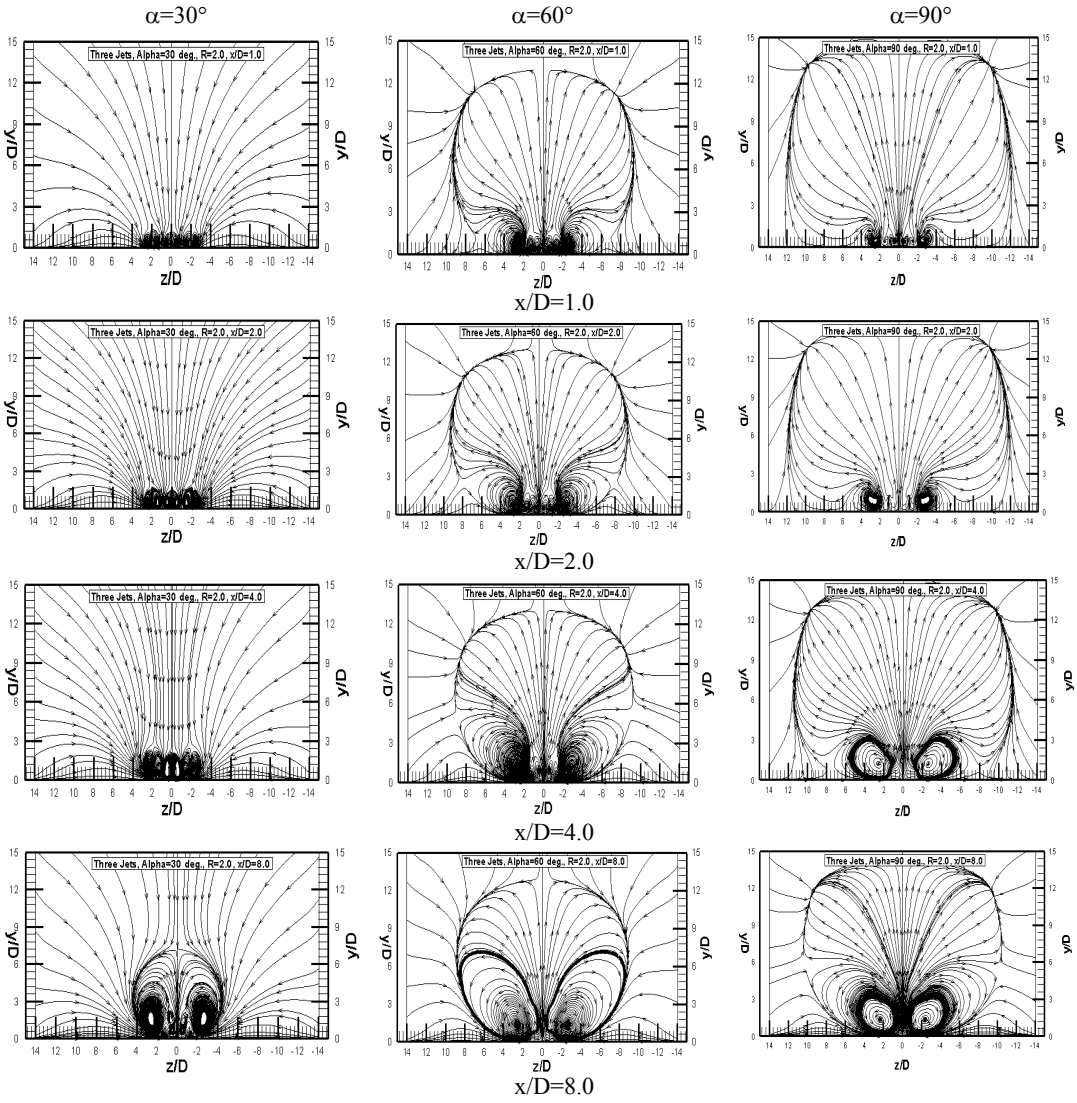

Fig. 8. CVP development at different inclination angles for three side-by-side nozzle arrangement, R=2.0.

channel. Although, it cannot be revealed in the present paper, Sakai *et al*. (2014) proposed the hanging and rear vortices play important roles for the development of the CVP especially at high velocity ratios.

Fig. 8 shows the cases of the three side-by-side circular cross-sectional nozzles. Vortex pairs that formed at the sides of the channel are merged with other vortex pair generated at the center of channel (main CVP) formed to be only one CVP as reported by Kolar and Savory, 2007. This is an expected result because the strong interaction of inner vortices rapidly canceling each other. CVP generated from circular cross-sectional three side-by-side nozzles are more strength than the one from the single nozzle shown in Fig. 7. The downstream development of circulation is dependent on the nozzle arrangement. Three side-by-side oriented nozzles introduce higher scale vortices into the flow compared to the single one. It is indicated that the three side-by-side jets move closer to the upper wall of the channel both in the near and far fields.

In case of three side-by-side nozzle the CVP collapses into a single vortex. It should be noted here that the development of CVP refers to a progression from distorted structures to the kidney-like shapes. Regardless of the inclination angles and the number of the nozzles, the vortex structure is more distorted especially at higher angles. This distortion leads to form significantly larger CVP in size and strength. Outer parts of CVPs are larger than the inner parts. CVP formed at the lowest velocity ratio (R) is the weakest and the smallest in size and hardly recognized. It is also depicted that as R increases the CVPs become stronger and the vortex centers move in the both directions. When R increases CVPs become strong enough to effect the formation of the secondary CVP near the wall

4. CONCLUSION

In the present paper, the effects of inclination angles on the development of CVP are analyzed

numerically for velocity ratio of R=2.0 after a series of successful validations with available experimental data for R=1. and R=2.0. s and inclination angles. In addition to the single nozzle jet flows are obtained by means of three side-by-side positioned circular nozzles. Enhancement of these parameters causes higher jet penetration into the channel and increases the lateral spreading of jets and CVPs in size.

REFERENCES

Andreopoulos, J. and W. Rodi (1984). Experimental investigation of jets in a crossflow *Journal of Fluid Mechanics 138, 93-127.*

Bayraktar, S. and T. Yilmaz (2008). Two-dimensional numerical investigation of film cooling by a cool jet injected at various angles for different blowing ratios, *Proceedings of the Institution of Mechanical Engineers Part C-Journal of Mechanical Engineering Science* 222(7), 1215-1224.

Bayraktar, S. and T. Yilmaz (2011). Three-dimensional analysis of temperature field for various parameters affect the film cooling effectiveness, *Energy Conversion and Management* 52(4), 1914-1929.

Bulat, M. P. and P. V. Bulat (2013). Comparison of turbulence models in the calculation of supersonic separated flows, *World Applied Sciences Journal* 27, 1263-1266.

Cable, M. (2009). *An evaluation of turbulence models for the numerical study of forced and natural convective flow in atria*, *MSc thesis,* Queen`s University, Kingston, Ontario, Canada.

Coletti, F., M. J. Benson, J. Ling, C. J. Elkins and J. K. Eaton (2013). Turbulent transport in an inclined jet in crossflow. *International Journal of Heat ad Fluid Flow* 43, 149-160.

Cortelezzi, L. and A. R. Karagozian (2001). On the formation of the counter-rotating vortex pair in transverse jets. *Journal of Fluid Mechanics*, 446, 347-373.

Demuren, A. O. and W. Rodi (1987). Three-dimensional numerical calculations of flow and plumes spreading past cooling towers. *Journal of Heat Transfer* 109(1), 113-119.

Foster, L. E. and W. A. Engblom (2003*). Computation of transverse injection into supersonic crossflow with various injector orifice geometries*. NASA/TM-2003-212878.

Fric, T. F. and A. Roshko (1989). Structure in the near field of the transverse jet. *7th Symposium on Turbulent Shear Flows*. Stanford CA, August 21-23(1), 6.4.1-6.4.6.

Fric, T. F. and A. Roshko (1994). Vortical structure in the wake of a transverse jet. *Journal of Fluid Mechanics* 279, 1-47.

Fuller, E. J. and R. W. Walters (1991). Navier-Stokes calculations for 3D gaseous fuel injection with data comparisons*. AIAA In: 3rd International Aerospace Planes Conference*, Orlando FL, Dec. 3-5.

Guo, X., W. Schröder and M. Meinke (2006). Large-eddy simulations of film cooling flows. *Computers and Fluids* 35, 587-606.

Hatch, M. S., W. A. Sowa, G. S. Samuelsen and J. D. Holdeman (1995). Geometry and flow influences on jet mixing in a cylindrical duct. *Journal of Propulsion and Power* 11(3), 393-402.

Hatch, M.S, Sowa, W.A., Samuelsen, G.S. (1992). *Influence of geometry and flow variation on jet mixing and NO formation in a model staged combustor mixer with eight orifices*. NASA CR 189094.

Haven, B. A. and M. Kurosaka (1997). Kidney and anti-kidney vortices in crossflow jets. *Journal of Fluid Mechanics* 352, 27-64.

Huang, W. (2015). Effects of jet-to-crossflow pressure ratio arrangement on turbulent mixing in a flowpath with square staged injectors. *Fuel* 144, 164-170.

Kalifa, R. B., S. Habli, N. M. Said, H. B. Bournot and G. L. Palec (2014). numerical and experimental study of a jet in a crossflow for different velocity ratio. *Journal of the Brazilian Society of Mechanical Sciences and Engineering* 36, 743-762.

Kamotani, Y. and I. Greber (1972). Experiments on a turbulent jet in a cross flow. *AIAA Journal* 10(11), 1425-1429.

Kelso, R. M., T. T. Lim and A. E. Perry (1996). An experimental study of round jets in cross-flow. *Journal of Fluid Mechanics* 306, 111-144.

Kolar, V. and E. Savory (2007). Dominant flow features of twin jets and plumes in crossflow. *Journal of Wind Engineering and Industrial Aerodynamics* 95(9-11), 1199-1215.

Margason, R. J. (1993). Fifty years of jet in cross flow research. *Proceedings of NATO AGARD Conference,* CP-534, Winchester, UK 1.1-1.11.

Marzouk, Y. M. and A. F. Ghoniem (2007). Vorticity structure and evolution in a transverse jet. *Journal of Fluid Mechanics* 575, 267-305.

Renze, P., W. Schröder and M. Meinke (2008). Large-eddy simulation of film cooling flows with variable density jets. *Flow, Turbulence and Combustion* 80(1), 119-132.

Rowbury, D. A., M. L. G. Oldfield and G. D. Lock (2001). Large-scale testing to validate the influence of external crossflow on the discharge coefficients of film cooling holes. *Journal of Turbomachinery* 121(3), 593-600.

Sakai, E., T. Takahashi and H. Watanabe (2014).

Large-eddy simulation of an inclined round jet issuing into a crossflow. *International Journal of Heat and Mass Transfer* 69, 300-311.

Shih, T. H., W. W. Liou, A. Shabbir, Z. Yang and J. Zhu (1995). A new k-ε eddy-viscosity model for high Reynolds number turbulent flows-model development and validation. *Computer and Fluids* 24(3), 227-238.

Tomioka, S., L. S. Jacobsen and J. A. Schetz (2003). Sonic injection from diamond-shaped orifices into a supersonic crossflow. *Journal of Propulsion and Power* 19(1), 104-114.

Tyagi, M. and S. Acharya (2003). Large eddy simulation of film cooling flow from an inclined cylindrical jet. *Journal of Turbomachinery* 125, 734-742.

Wang, C. R. (2000). Application of a turbulence model for jet and cross flow interaction. *Fluids 2000 Conference and Exhibit*, Denver, CO, June 19-22.

Williams, S. and R. Hartfield (1996). An analytical investigation of angled injection into a compressible flow. *32nd ASME, SAE and ASEE, Joint Propulsion Conference and Exhibit*, Lake Buena Vista, FL, July-1-3.